

Observations of Aerosol-Vapor Pressure Deficit-Evaporative Fraction coupling over India

Chandan Sarangi^{1,2,7*}, Tirthankar Chakraborty^{3,4}, Sachchidanand Tripathi^{1,3*}, Mithun Krishnan¹,
Ross Morrison⁵, Jonathan Evans⁵, Lina Mercado^{5,6}

Affiliations:

¹ Department of Civil engineering, Indian Institute of Technology Madras, Chennai, India

² Department of Civil engineering, Indian Institute of Technology Kanpur, Kanpur, India

³ Center for Environmental Science and Engineering, Indian Institute of Technology Kanpur,
India

⁴ School of the Environment, Yale University, US

⁵ UK Centre for Ecology & Hydrology, Wallingford, UK

⁶ Department of Geography, University of Exeter, UK

⁷ Laboratory of Atmospheric and Climate Sciences, Indian Institute of Technology Madras,
Chennai, India

* Corresponding authors:

Sachchidanand Tripathi: snt@iitk.ac.in

and

Chandan Sarangi: chandansarangi@iitm.ac.in

Abstract

North India is a densely populated subtropical region with heavy aerosol loading (mean Aerosol Optical Depth or AOD ~ 0.7), frequent heatwaves and strong atmosphere-biosphere coupling, making it ideal for studying the impacts of aerosols and temperature variation on latent heat flux (LH) and evaporative fraction (EF). Here, using in situ observations during the onset of the summer monsoon over a semi-natural grassland site in this region, we confirm that strong co-variability exists among aerosols, LH, air temperature (T_{air}) and vapor pressure deficit (VPD). Since the surface evapotranspiration is strongly controlled by both physical (available energy and moisture demand) and physiological (canopy and aerodynamic resistance) factors, we separately

32 analyze our data for different combinations of aerosols and $T_{\text{air}}/\text{VPD}$ changes. We find that
33 aerosol loading and warmer conditions both reduces SH. Further, we find that an increase in
34 atmospheric VPD, tends to decrease the gross primary production (GPP) and thus LH, most
35 likely as a response to stomatal closure of the dominant grasses at this location. In contrast, under
36 heavy aerosol loading, LH is enhanced partly due to the physiological control exerted by the
37 diffuse radiation fertilization effect (thus increasing EF). Moreover, LH and EF increases with
38 aerosol loading even under heatwave conditions, indicating a decoupling of plant's response to
39 VPD enhancement (stomatal closure) in presence of high aerosol conditions. Our results
40 encourage detailed in situ experiments and mechanistic modelling of AOD-VPD-EF coupling for
41 better understanding of Indian monsoon dynamics and crop vulnerability in a heat stressed and
42 heavily polluted future India.

43

44 **Highlights:**

- 45 1. A rigorous analysis of Aerosol-EF-VPD coupling using collocated direct observations is
46 presented
- 47 2. Increased aerosol loading enhances Evaporative Fraction by decreasing sensible heat and
48 increasing latent heat.
- 49 3. Aerosols modulate the response of vegetation to changes in VPD under heatwave conditions

50

51 **Keywords:** Grassland, Aerosol loading, eddy covariance, evaporative fraction, physiological
52 response, diffuse radiation, Indo Gangetic Plains, heatwave, sensible heat, latent heat, Bowen
53 ratio

54

55

56 **Introduction:**

57 The surface energy balance represents the balance between the net radiation (NR) flux at
58 the Earth's surface and the partitioning of NR into latent heat (LH), sensible heat (SH) and
59 ground heat (GH) fluxes [Wang and Dickinson, 2012]. While the dominant partitioning of
60 energy as SH enhances the near-surface air temperature, the LH flux cools the surface and
61 increases the moisture content of the boundary layer. Thus, perturbations to the partitioning of

62 the outgoing turbulent energy fluxes from the land surface modify the near surface
63 micrometeorology. One way of representing this partitioning is the evaporative fraction
64 ($EF=LH/(SH+LH)$), or the proportion of the total available energy ($NR-GH$) available at the
65 surface released via vegetation evapotranspiration and soil evaporation. Earlier studies have
66 established that the EF can be modulated by a range of factors, including vapor pressure deficit
67 (VPD), soil moisture, canopy structure, atmospheric composition, solar radiation and stomatal
68 behaviour [Baldocchi, 1997; Wilson et al., 2002].

69 The variability in VPD, which describes the near surface moisture deficit for a given
70 temperature (difference between the saturated and ambient vapor pressure for atmospheric water)
71 is arguably the dominant nonlinear forcing on EF variability [Gu et al., 2006]. On one hand, an
72 increase in VPD leads to the partitioning of more of the available energy into LH to meet the
73 atmospheric moisture demand, part of the physical control on evapotranspiration [Penman, 1948;
74 Monteith et al., 1965]. On the other hand, high VPD also triggers partial closure of leaf stomata
75 in response to increased atmospheric dryness [Jones and Sutherland, 1991; Damour et al., 2010;
76 Medlyn et al., 2011]. This is part of the physiological control on ET, causing an increase in VPD
77 to actually decrease ET (and thus EF) [Rigden & Salvucci, 2017]. Moreover, the sign of VPD-
78 EF association could also change due to variations in confounding factors like ambient soil
79 moisture and diffuse/direct radiation [Gu et al., 2006]. More diffused radiation enhances plant
80 productivity [Mercado et al., 2009; Rap et al., 2018] and plant growth [Wang et al., 2018];
81 which, in turn, can increase LH and EF [Chakraborty et al., 2021; Davin et al., 2012; Wang et al.,
82 2008]. However, this association is also reported to have an optimum point beyond which plant
83 productivity declines with increasing diffused fraction of radiation [Knohl et al., 2008].

84 Small particles suspended in the atmosphere, i.e. atmospheric aerosols, can alter the
85 amount of shortwave and longwave radiation reaching the surface, through scattering and
86 absorption, thereby altering NR [Schwartz, 1996; Trenberth et al., 2009; Chakraborty and Lee,
87 2019]. This is commonly known as the aerosol direct radiative effect (ADRE) and is dependent
88 on aerosol size, composition and vertical distribution in the atmosphere [Forster et al., 2007;
89 Sarangi et al., 2016]. Global and regional scale modelling studies have reported that the ADRE
90 can greatly alter the surface fluxes and microclimate over land [Liu et al., 2014; Mallet et al.,
91 2009; Shen et al., 2020; Myhre et al., 2018]. Generally, the ADRE reduces NR, which results in

92 the reduction in the magnitude of SH and LH. But, loading of scattering aerosols from fossil fuel
93 combustion can also increase the diffuse fraction of solar radiation at the surface, which affects
94 the photosynthesis and LH or EF [Chameides et al., 1999; Matsui et al., 2008; Niyogi et al., 2004;
95 Wang et al., 2008; O'Sullivan et al., 2016; Wang et al., 2020]. This mechanism is generally
96 referred to as the diffuse radiation induced aerosol fertilization effect (ADFE). But, depending on
97 the ecosystem, the positive association of ADFE on EF also gets saturated as ADRE becomes
98 larger than a threshold [Yue et al., 2017]. Further, Steiner et al., [2013] reported that warmer air
99 temperature are consistent with high aerosol optical depth (AOD) scenario over various in-situ
100 micrometeorological sites in USA, which can result in no clear association between AOD and
101 LH. Thus, how aerosol loading modulates the already complex VPD-EF association can depend
102 on the interplay between radiation, ADFE, aerosol amount and properties, background climate
103 and ecosystem phenology [Steiner et al., 2011].

104 Northern India is a global hot spot for atmospheric aerosols with AOD varying between 0.5 and
105 1.5, and high aerosol radiative efficiency values ($\sim 100 \text{ W/m}^2/\text{AOD}$) during pre-monsoon period
106 [Dey et al., 2011; Kumar et al., 2015; Dimitris et al., 2012; Sarangi et al., 2016; Srivastava et al.,
107 2011]. In addition, the region also experiences frequent high temperature days and heatwave
108 conditions, generally extending for 2-6 days during this period [Ratnam et al., 2016; Rohini et
109 al., 2016]. During heatwave conditions, the regional atmosphere is largely stagnant [Ratnam et
110 al., 2016], which can lead to greater air temperature by 5-10 K and magnifies the water vapour
111 demand by 2-3 times at weekly time scale. In addition to high air temperatures (T_{air}), high
112 aerosol loading during heatwaves have also been reported over Northern India [Dave et al., 2020;
113 Mondal et al., 2020] at this time of year. Moreover, the value of EF is typically greater than 0.5
114 over the Northern India during pre-monsoon period, indicating a potentially larger control of
115 VPD-LH linkages on surface energy partitioning [Bhat et al., 2019]. Steep variability in ambient
116 values of VPD (also AOD in some events) during heatwaves over Northern India provides us
117 with ideal conditions for investigating the associations between aerosol loading and VPD-EF
118 coupling.

119

120 Previous studies have suggested that aerosol loading can modulate the partitioning of surface
121 fluxes over Northern India [Urankar et al., 2012; Murthy et al., 2014; Latha et al., 2019; Gupta et

122 al., 2020]. However, these studies have been based on reanalysis products [Urankar et al 2012],
123 very limited measurements of SH only [Murthy et al., 2014] or estimated derived from remotely
124 sensed data [Latha et al., 2019] and therefore lack the fidelity that can be obtained from direct
125 observations of key processes. Better understanding of the aerosol-VPD-EF associations using
126 direct collocated observations is essential to understand present day conditions and potential
127 feedbacks that can modify future climate over this region of great hydro-climatic significance. In
128 this study, we have used co-located observations of surface energy balance, near-surface
129 micrometeorological variables and soil characteristics, together with aerosol properties (both
130 surface and columnar) at a sub-tropical site in northern India during the pre-monsoon season.
131 Analysis of case studies with AOD varying in phase or remaining constant with high VPD
132 (under heatwave conditions) are done to understand the underlying processes. Here, we will
133 present compelling evidence that changes in EF is directly (indirectly) proportional to aerosol
134 loading (VPD). More interestingly, we found that aerosol loading can decouple the observed
135 strong VPD-LH relationship under heatwave scenario which can have serious implications on
136 climate resilience of crops and vegetation. Below, the sections are organized to discuss the data
137 used, case studies selected and methodology, results, discussions and summary of this study.

138

139 **2. Observation site and data:**

140

141 Observations of SH, LH and net ecosystem CO₂ exchange (NEE) were obtained over a
142 semi-natural grassland site (Figure 1A) within the campus of the Indian Institute of Technology,
143 Kanpur (IITK; 26.5N, 80.3E, elevation 132 m above mean sea level) during the pre-monsoon
144 months (April-June) of 2016-2017. Energy flux data were collected by an eddy covariance
145 system installed at 5.28 m above the soil surface. This flux measurement site is part of an eddy
146 covariance network set up in India as part of the INCOMPASS project of the Indo-UK Monsoon
147 Programme [Chakraborty et al., 2019; Turner et al. 2019; Bhat et al., 2019]. The eddy covariance
148 system consists of a Windmaster sonic anemometer-thermometer (Gill Instruments Ltd.
149 Lymington, UK) and a LI7500 infrared gas analyzer (LI-COR Biosciences, Logan, Utah, USA).
150 The fetch around the tower is a mixture of different C₄ grasses, i.e. variants of Napier grass
151 (~60-70%) and some common reed (Scientific family: Pennisetum purpureum and Phragmites-
152 Saccharum-Imperata). Napier grasses are invasive and a perennial species and representative of

153 grasslands in the region (Chakraborty et al., 2019; Holm et al., 1979). The vegetation cover is
154 more than 90% of the fetch of the flux tower (Figure 1B) and the canopy height varied within 1-
155 1.5 m during our study periods. The soil is typical of the Gangetic Plains with silt, clay and sand
156 fractions of 80%, 15% and 5%, respectively (unpublished data). The site experiences a humid
157 subtropical climate. The range in daily AOD and T_{air} was 0.4-1.4 and 32-45 °C, respectively,
158 during the study period (Figure 1C).

159
160 The net radiation (NR; W m^{-2}) and its incoming and outgoing short- and longwave
161 components were measured using an NR01 net radiometer (Hukesflux, Delft, The Netherlands)
162 installed at 5 m above the surface. The surface temperature (T_{srf}) was calculated from the
163 measured outgoing longwave radiation following the Stefan–Boltzmann law assuming an
164 emissivity of 0.95 [Trenberth et al., 2009]. Ground heat fluxes (GH; W m^{-2}) were monitored at
165 0.03 m below the soil surface using two HFP01-SC self-calibrating soil heat flux plates
166 (Hukesflux, Delft, The Netherlands). Near surface air temperature (T_{air} ; °C) and relative humidity
167 (RH; %) were measured at a height of 4.5 m. Wind speed and wind direction were measured at
168 10 m above the soil surface using a WindSonic anemometer (Gill Instruments Ltd., Lymington,
169 UK). Volumetric soil water content (VWC; m^3 of water in m^3 of soil) and surface temperature
170 (T_{srf} ; °C) were measured using two pairs of digital TDT sensors (Acclima Inc., Meridian, Idaho,
171 USA) installed at 0.05 and 0.15 m below the soil surface. Standard data processing and quality
172 control routines were used to calculate surface fluxes as described in Morrison et al. 2019. Data
173 gap-filling and the partitioning of net ecosystem exchange into Gross Primary Production (GPP)
174 and total ecosystem respiration was performed using the R EddyProc package [Reichstein et al.,
175 2016; Reichstein et al., 2005]. Negative net ecosystem exchange during the daytime period
176 indicates that photosynthesis at our site dominates over soil and plant respiration (not shown).
177 Since water and carbon cycles in the plants are closely coupled [Collatz et al., 1991]; variations
178 in GPP are used as a proxy for plant transpiration in this study. More details on the flux, weather
179 and radiation tower measurements at IIT Kanpur can be found in Table S1 and Chakraborty et
180 al., 2019.

181

182 Version 2 instantaneous cloud screened (Level 1.5) half-hourly averages of Aerosol
183 Optical Depth (AOD) at 550 nm and Single Scattering Albedo (SSA), the ratio of scattering
184 efficiency to total extinction efficiency, at 440 nm obtained from the AErosol RObotic NETwork
185 (AERONET) station deployed in the IITK campus (Figure 1A) were used to quantify the aerosol
186 optical properties during our study period. Low and high SSA values indicate dominance of
187 absorbing and scattering aerosols in the column, respectively. Clear-sky short wave (0.25–4 μ m)
188 radiative transfer calculations, using the Santa Barbara discrete ordinates radiative transfer
189 Atmospheric Radiative Transfer Model (SBDART) [Ricchiazzi et al., 1998], are used to estimate
190 the midday aerosol direct radiative forcing (ADRF) at surface and diffuse radiation reaching the
191 surface ($\text{diffuse}_{\text{frac}}$). Midday mean AOD and SSA for each day are prescribed to the model.
192 More details on radiative flux calculations using SBDART are mentioned in Supplementary
193 Information file. Finally, micro-pulse lidar backscatter images (Level 1.5) measured at the
194 collocated Micro-Pulse Lidar Network site [Campbell et al., 2002; Welton and Campbell, 2002]
195 are also used in this study, mainly to identify cloudy days. A day is termed as a cloudy day if
196 cloud patches are observed in Lidar profiles for more than 3 hours. More details on the aerosol
197 measurements can be found in supplementary information file.

198

199 **3. Case studies and methodology:**

200

201 In order to examine the impact of aerosols or VPD on EF, we need to carefully identify
202 periods where the variability of other confounding factors is negligible. As such, we identified
203 three weeks (marked in Figure 1C) for analysis, where daily variations in all these factors except
204 T_{air} /VPD and AOD is negligible. Figure 1C illustrates the occurrences of cloudy days, rainfall
205 and wildfire-affected periods during pre-monsoon months of 2016 and 2017. We have avoided
206 periods of cloud and rainfall occurrences since that would affect the surface and energy budget
207 much more than the ADFE. The daily mean VWC values are also shown for the period in Figure
208 1C. However, as shown in Figure 1C, it is rare to have a considerable time interval with only
209 variation in AOD values (and negligible variation in T_{air} /VPD). Eventually, three one-week
210 periods are carefully selected with different combinations of dominant weekly gradients in T_{air}
211 /VPD and AOD and analyzed to gain insights into ambient AOD-VPD-EF association. The first
212 week selected for analysis is between 2nd-9th June, 2016, which had high weekly gradient in

213 AOD but was accompanied by low variation in $T_{\text{air}}/\text{VPD}$ (hereafter referred as High AOD-Low
214 T_{air} (HALT) case). The second week is during 10th-15th April, 2017, which witnessed large daily
215 increase in aerosol loading as well as T_{air} in phase throughout the week (hereafter referred to as
216 the High AOD-High T_{air} (HAHT) case). We also selected a third week during 10th-15th May,
217 2017, when high gradient in T_{air} was observed across the week, but negligible weekly gradient in
218 AOD was present i.e the AOD values had large day to day variability through the week
219 (hereafter referred to as the Low AOD- High T_{air} (LAHT) case). Interestingly, heatwave
220 conditions were prevalent over North India during the HAHT and LAHT weeks, therefore, a
221 wide range of VPD-AOD-EF variation can be sampled. Moreover, since there were no rainfall
222 events during these three weeks, the variation in VWC was minor compared to large daily
223 variations in T_{air} and AOD during our study periods. Further, the variations in the vegetation
224 phenology, wind and boundary layer height are found to be negligible within each of these three
225 weeks. Note that no week with low AOD and low VPD variations was observed during our study
226 period.

227 The simultaneous midday (1000-1500 LT) variability in AOD, VPD, EF and the other
228 components of the surface radiative balance is analyzed across the HALT and LAHT weeks to
229 understand the impact of strong weekly gradients of AOD and VPD, respectively. Further, we
230 analyse the weekly gradients in the observations during HAHT, and compare and contrast the
231 same with the HALT and LAHT cases to understand the combined effects of AOD and VPD.

232 Moreover, to examine the impact of aerosol loading on VPD-EF associations under enhanced
233 heat stress, we also calculated the daily midday bulk canopy resistances for both HAHT and
234 LAHT cases by inverting the Penmann-Monteith equation as described below. We used observed
235 values of available energy, VPD, T_{srf} derived from observed LW_{out} , psychrometric constant and
236 slope of vapor pressure curve derived from observed surface pressure and T_{air} respectively, and
237 aerodynamic resistance derived from the observed SH and near-surface temperature gradient.

238 The aerodynamic resistance to heat transfer (r_a) is calculated from the near-surface temperature
239 gradient and the measured distance between the two (H), given by:

$$240 \quad r_a = \frac{-\rho C_p (T_{\text{srf}} - T_{\text{air}})}{H}$$

241 where T_{srf} is the surface temperature, calculated by inverting the Stefan-Boltzmann law assuming
 242 a unit surface emissivity (reasonable for vegetated surfaces), ρ is the air density, and C_p is the
 243 specific heat at constant pressure ($1.005 \times 10^{-3} \text{ MJ kg}^{-1} \text{ }^\circ\text{C}^{-1}$).

244 Then, the canopy resistance (r_s) is calculated by inverting the Penman-Monteith approximation.
 245 Thus:

$$246 \quad r_s = \frac{\frac{\Delta(Rn - G) + \frac{\rho C_p VPD}{r_a}}{LE} - \Delta}{\gamma - 1} r_a$$

247 where Δ is the slope of the water vapor saturation curve given by:

$$248 \quad \Delta = \frac{4098 [0.6108 \exp(\frac{17.27 T_a}{T_a + 237.3})]}{(T_a + 237.3)^2}$$

249 and γ is the psychrometric constant, calculated as:

$$250 \quad \gamma = \frac{C_p P}{\epsilon \lambda}$$

251 where P is atmospheric pressure in kPa, λ is the latent heat of vaporization (2.45 MJ kg^{-1}), and ϵ
 252 is the ratio of the molecular weight of water vapour to dry air (0.622).

253 **4. Results:**

254 During the HALT period, midday AOD values decreased monotonically across the week from
 255 ~ 1.1 on 2nd June, 2016 to ~ 0.6 on 9th June, 2016 (Figure 2A). The corresponding trend in SSA
 256 values was negligible, but SSA values are ~ 0.92 indicating a predominance of scattering aerosols
 257 (Figure 2A). Corresponding values of NR at surface increased monotonically by $\sim 50 \text{ W/m}^2$
 258 during the same week (Figure 2D). The enhancement in midday NR with decreasing AOD is
 259 strongly driven by the corresponding increase in midday incoming shortwave radiation (ISWR)
 260 by $\sim 100 \text{ W/m}^2$ (Figure 2D). In agreement, ADRF values at surface decreased by $\sim 80 \text{ W/m}^2$ and
 261 diffuse fraction of incoming radiation increased by ~ 0.10 with decrease in scattering aerosols
 262 from 2nd June to 9th June, 2016 (Figures S1A and S1D). The daily trend in modelled ADRF (and
 263 diffused fraction) values are consistent with the daily reduction trend of ISWR during HALT,

264 reinforcing the expectation that negative daily trend in ISWR and NR during HALT was
265 primarily by aerosol-induced radiative changes.

266
267 During HAHT, the midday AOD values increased monotonically across the week from
268 ~ 0.3 on 10th-11th April to ~ 0.8 on 14th-15th April (Figure 2B). Corresponding values of NR and
269 ISWR at surface decreased monotonically by $\sim 100 \text{ W/m}^2$ and $\sim 200 \text{ W/m}^2$, respectively, during
270 the same period (Figure 2E). Similar to HALT, no daily trend was present in SSA values during
271 HAHT and SSA values are ~ 0.9 indicating presence of scattering aerosols (Figure 2B). In
272 agreement, ADRF values at surface decreased across the week (Figure S1B) with highest values
273 on high AOD days (14th-15th April; $\sim 150 \text{ W/m}^2$) compared to those on low AOD (10th-11th April;
274 $\sim 50 \text{ W/m}^2$). At the same time, the diffuse fraction of incoming radiation at the surface (Figures
275 S1E) increased substantially from ~ 0.5 (on 10th April) to ~ 0.7 on (15th April) during HAHT
276 indicating strong impact of aerosol loading.

277
278 In contrast, during LAHT week, the gradient of AOD values from 10th and 15th May, 2017 was
279 relatively minor (Figure 2C). As the increase in AOD through the week was smaller compared to
280 other two cases, corresponding decrease of NR and ISWR values at surface was also smaller in
281 magnitude ($\sim 30 \text{ W/m}^2$) during this period (Figure 2F). Correspondingly, negligible trend in
282 ADRF (Figures S1C) at the surface is observed indicating low variation in aerosol radiative
283 effect change during the LAHT week. Moreover, the midday SSA values during LAHT are
284 lower (~ 0.8) compared to HALT and HAHT cases indicating presence of highly absorbing
285 aerosols in the column (Figure 2C). Accordingly, the ADRF values at surface during LAHT
286 (Figure S1C) were very high, more than double of the same during HALT and HAHT (i.e. ~ 350
287 W/m^2). This can be explained by the fact that absorbing aerosols (lower SSA values) were
288 relatively dominant during LAHT compared to the other 2 cases. Moreover, dominance of
289 absorbing aerosols also lead to minor variation in diffused radiation during the week (Figure
290 S1F). To sum up, the impact of aerosol variability (i.e. the gradient in direct radiative effect and
291 diffused fraction modulation) is minor during the week compared to HAHT and HALT weeks.

292

293 As aerosol direct radiative effect induces surface cooling, midday T_{srf} values reduced
294 from $\sim 35^{\circ}\text{C}$ during low AOD days to $\sim 30^{\circ}\text{C}$ during high AOD days across the HALT week
295 (Figure 3A). At the same time, the variability in T_{air} values remain more or less constant during
296 HALT. Therefore, the midday variation of temperature difference between T_{srf} and T_{air} ($\Delta T = T_{\text{srf}}$
297 $- T_{\text{air}}$) is inversely proportionally with aerosol loading for HALT (Figure 3A). Greater the value
298 of ΔT , greater will be the turbulent and convection flux, and greater is the tendency of SH flux
299 release at surface. Consequently, sensible heat fluxes are also inversely proportional to increase
300 in AOD (and aerosol direct effect). With increase (decrease) in ΔT (AOD) values, the
301 corresponding SH values increased linearly from $\sim 60 \text{ W/m}^2$ on 2nd June to $\sim 120 \text{ W/m}^2$ on 9th
302 June, 2016 during HALT week (Figure 3D).

303
304 By contrast, a distinct and steep increase in midday T_{air} ($\sim 10^{\circ}\text{C}$) is seen during HAHT
305 and LAHT weeks. Correspondingly, the mid-day T_{srf} values are also seen to be increasing in
306 close coupling with the T_{air} values during these two weeks (Figures 3B-C). This coupling is
307 mainly because of the coexisting stagnant scenario under heatwave periods. Nonetheless, ΔT
308 variation is inversely proportional to AOD variation during both the weeks (Figure 3B-C).
309 Because, some portion of the enhancement in midday T_{srf} is compensated by the aerosol-induced
310 surface cooling, steeper AOD trend across the week means greater ΔT magnitude. For instance,
311 as aerosol radiative effect is relatively smaller across the week during LAHT compared to that
312 during HAHT, a relatively larger decrease in daily ΔT ($> 2^{\circ}\text{C}$) is observed during HAHT week
313 (Figure 3B). Consistently, the magnitude of SH also significantly decreased across the week in
314 HAHT and LAHT. Specifically, the midday mean values of SH decreased linearly from ~ 200
315 W/m^2 on 10th April (low AOD) to $\sim 100 \text{ W/m}^2$ on 15th April, 2017 (high AOD) during HAHT
316 (Figure 3E). During LAHT, the midday mean SH decreased linearly from $\sim 200 \text{ W/m}^2$ on 11th
317 May to $\sim 125 \text{ W/m}^2$ on 14-15th May, 2017 (Figure 3F).

318
319 The midday latent heat values decreases by $\sim 150 \text{ Wm}^{-2}$ from high AOD days to low
320 AOD days during HALT week (Figure 3D). In comparison, the increase in LH values with
321 increase in AOD across the HAHT week from 10th April, 2017 to 15th April, 2017 is gradual i.e.
322 $\sim 25 \text{ W/m}^2$ (Figure 3E). Specifically, the slope of regression of latent heat against AOD is 70
323 $\text{W/m}^2/\text{AOD}$ and $10 \text{ W/m}^2/\text{AOD}$ for HALT and HAHT cases, respectively (figure not shown).

324 As, VPD values increase steeply in HAHT case (Figure 3H), but no distinct variation in VPD
325 across the week was evident for HALT case (Figure 3G). Examination of corresponding midday
326 values of gross primary production (GPP) flux (Figures 3G-F) also illustrate gradients similar in
327 sign to corresponding latent heat fluxes indicating that the daily variation in LH flux in both the
328 cases is mainly due to associated variation in evapotranspiration. Keeping in mind that the
329 magnitude of AOD variation in both the above cases are similar, the differences in slopes of LH-
330 AOD regression (lower value during HAHT) could be attributed to the simultaneous suppression
331 of evapotranspiration by VPD rise during HAHT week.

332

333 VPD-associated decline in GPP and thus LH fluxes is even more clearly observed during
334 LAHT week. A strong negative trend in midday values of latent heat and GPP is observed as the
335 week progressed from low to high VPD during LAHT (Figure 3F and 3I). Quantitatively, the
336 slope of regression of (midday mean) latent heat against T_{air} is $+4.1 \text{ W/m}^2/\text{°C}$ and $-6.6 \text{ W/m}^2/\text{°C}$
337 for HAHT and LAHT cases, respectively. Note that the magnitude of VPD variation in both the
338 cases is similar, so the differences in slope of latent heat and T_{air} regression can be attributed to
339 the corresponding differences in aerosol loading. Thus, the magnitude of latent heat or GPP is
340 directly proportional to changes in magnitude of AOD (as seen in HALT), but the same is
341 inversely proportional to variations in T_{air} or VPD (as seen in LAHT), and the net effects can
342 largely compensate each other (as seen in HAHT).

343

344 Moreover, the gradient in EF was substantial only in HAHT and HALT where there was
345 substantial variation in AOD across the week. Partitioning of surface energy into latent heat or
346 the latent heat fraction (LHF: Latent heat / Net radiation) decreased and that into sensible heat
347 fraction (SHF: Sensible heat / Net Radiation) increased with increase in AOD across the week
348 during HALT (Figure 3J). As a result, the midday EF distribution decreased with reduction in
349 AOD from ~ 0.8 on 2nd June to ~ 0.6 on 9th June during HALT (Figure 3J). On the same line,
350 with increase in AOD across the week during HAHT, EF also increased from ~ 0.63 on 10th
351 April, 2017 to ~ 0.78 on 15th April, 2017 (Figure 3K) due to simultaneous decrease and increase
352 in SHF and LHF, respectively. But, in absence of clear aerosol gradient across the week, no
353 substantial variation was observed in EF across the week during LAHT case (Figure 3L). The
354 decrease in sensible heat with VPD enhancement was similar in HAHT and LAHT cases (Figure

355 3K-L). But, LH release increased (decreased) with VPD during the former (later) case indicating
356 a role of AOD change on VPD-EF association.

357

358 Figure 4 illustrates the variation in midday mean canopy resistance during the LAHT and
359 HAHT weeks to various physical and physiological factors that control evapotranspiration,
360 namely moisture demand, available energy, air temperature and the aerodynamic resistance. As
361 expected, the canopy resistance is significantly ($p < 0.05$) correlated with VPD although clear
362 differences in the slope is present for the two cases. Specifically, the canopy resistance increases
363 steeply from 400 to 1400 $s\ m^{-1}$ with increase in VPD from 40 to 70 hPa during LAHT case
364 (Figure 4a). However, the canopy resistance only increases from 400 to 500 with an increase in
365 VPD from 45 to 65 hPa during HAHT case (Figure 4a). Similarly, air temperature during these
366 periods also shows a statistically significant positive relationship with canopy resistance (Figure
367 4d). However, during both periods, canopy resistance was found to be independent of available
368 energy (Figure 4c) and the aerodynamic resistance (Figure 4d), indicating that the sensitivity of
369 canopy resistance to changes in VPD (or T_{air}) is significantly greater than that for the other
370 variables.

371 The LAHT case illustrates the frequently reported behaviour of reduction of canopy
372 conductance under increasing VPD due to partial stomata closure as a physiological stress
373 response (Grossiord et al., 2020). Similar responses are also reported in Napier grasses, the
374 native vegetation over our site (Mwendia et al. 2016). Napier grasses can be anisohydric, i.e.
375 water spending under ample water availability (Cardoso et al., 2015). But their behaviour
376 becomes isohydric under high temperature and high water stress (Liang et al., 2017; Mwendia et
377 al. 2014; Purbajanti et al., 2012). During both HAHT and LAHT weeks, soil moisture is very
378 low, hence, the Napier grasses behaves isohydrically under high VPD. The comparison of LAHT
379 and HAHT scatter illustrates that canopy conductance is not strongly affected even under severe
380 VPD rise when aerosol loading also increases in phase. Specifically, the strong gradient of
381 increase in canopy resistance with VPD/ air temperature gets moderated under the high aerosol
382 scenario. Thus, under the presence of high aerosol loading, the isohydric response of Napier
383 grass to temperature rise or the physiological stress under high VPD is decoupled. This can
384 partially explain the aerosol-induced increase in EF (as well as LH and GPP) even under high
385 VPD rise during HAHT.

386 Further, meteorological co-variability or any significant differences in weekly pattern of
387 other micro-meteorological variables between HAHT and LAHT cases can also contribute to the
388 corresponding differences in AOD-VPD-EF association. A closer look illustrates that minor
389 gradients are present in the meteorological variables (Figure S2), which can have secondary
390 effects on the VPD-EF associations. Nonetheless, the individual or relative contribution of these
391 meteorological variability and aerosols on the observed coupling remains unknown and deserves
392 further attention in future studies with in depth mechanistic modelling.

393

394 **5. Discussion:**

395

396 The increase in scattering aerosols increased diffused radiation during HALT; thereby
397 facilitating relatively more photosynthesis and thus more GPP and latent heat release with
398 increase in AOD. At the same time, increase in AOD also decreased the temperature difference
399 between surface and air and constrained sensible heat release, eventually leading to aerosol-
400 mediated increase in EF during HALT. However, previous studies investigating the role of
401 aerosols on surface energy fluxes over India have largely reported that aerosol loading is
402 inversely related to latent heat [Murthy et al., 2014; Latha et al., 2019; Gupta et al., 2020].
403 Possible explanations for this apparent contradiction are as follows. First, these studies did not
404 explicitly account for the effect of daily meteorology/ VPD/ temperature variability in their
405 analysis which can have confounding effects (as shown here and discussed in Steiner et al.,
406 2013). Second, these studies were not focused on grassland. Murthy et al., 2014 used
407 micrometeorological site data with a forested footprint in Ranchi. At the same time, Latha et al.,
408 2019 performs analysis at 100 km spatial resolution from reanalysis product/Model, which is
409 representative of a composite land use (including cities, forest, cropland and grassland) and thus
410 a mixture of evapotranspiration and ground evaporation. Gupta et al., 2020 used
411 micrometeorological observations within a typical university canopy (buildings, roads and trees)
412 in Mumbai. Note that total LH can decrease due to aerosols and EF can still increase if SH is
413 decreasing more than EF due to reduction in available energy. Nonetheless, our finding of direct
414 proportionality between aerosol loading and latent heat (or photosynthesis) is consistent with

415 previously reported in-situ studies over grasslands sites in USA [Niyogi et al., 2004; Gu et al.,
416 2002; Wang et al., 2008].

417 In contrast, aerosol loading and heatwave conditions both suppressed sensible heat release.
418 Greater aerosol direct radiative effect induces more surface cooling (Chakraborty and Lee,
419 2019), and hence lower sensible heat fluxes (Yu et al., 2002; Urankar et al., 2012; Steiner et al.,
420 2013), as seen in HALT case. Simultaneously, sensible heat release is also directly proportional
421 to the near surface temperature gradient during Pre-monsoon (Rao et al., 2019), which is clearly
422 seen in LAHT case. In HAHT case, both the effects work in phase to suppress release of sensible
423 heat. The reduction of sensible heat per unit change of T_{air} is $8 \text{ W/m}^2/^{\circ}\text{C}$ during LAHT
424 compared to the same being $11 \text{ W/m}^2/^{\circ}\text{C}$ in HAHT case. At the same time, the reduction of
425 sensible heat per unit change of AOD is $135 \text{ W/m}^2/\text{AOD}$ during LAHT compared to the same
426 being $65 \text{ W/m}^2/\text{AOD}$ in HALT case. Hence, increase in AOD and T_{air} , both suppress the release
427 of available surface energy via sensible heat and the effect is largely additive. Moreover, the
428 intensity of the AOD-induced sensible heat suppression will be stronger if the aerosols are
429 composed of relatively more absorbing aerosols, specifically black carbon [Myhre et al., 2018].
430 Because, they not only cool the T_{srf} (Mallet et al., 2009; Pandithurai et al., 2008a; Shen et al.,
431 2020) but also can warm T_{air} (especially under stagnant/heatwave conditions), thereby reducing
432 the near surface temperature gradient and inducing lower tropospheric stability [Dave et al.,
433 2020; Steiner et al., 2013; Myhre et al., 2018].

434

435 However, contrary to our results, a recent modelling study over India reports that
436 enhancement of absorbing aerosols are positively associated with increase in sensible heat and
437 air temperature under heatwave scenario [Mondal et al., 2020]. The inherent model biases in the
438 aerosol properties and concentration as well as absence of detailed canopy-atmosphere processes
439 in the model simulations of Mondal et al., 2020 may cause differences in the signature of the
440 AOD-sensible heat feedback. At the same time, the above differences can also be explained by
441 taking into consideration the difference in time-scale of the feedback used in analysis. For
442 example, a robust positive association between morning time black carbon concentrations and
443 mid-day T_{air} is observed by Talukdar et al., 2020. Although, they attributed this association
444 primarily to diurnal evolution of the residual layer mixing, the understanding from our study can

445 also explain a possible pathway. High black carbon loading during morning time can suppress
446 instantaneous sensible heat release (via reduction in the near surface temperature gradient),
447 followed by release of the additional sensible heat amount in the mid-day period under relatively
448 unstable atmosphere (and lower black carbon concentration due to dilution effect). As such,
449 correlations between absorbing aerosols and sensible heat at instantaneous scale can be negative
450 (as seen in HAHT), but correlations or composite analysis at daily or monthly time scale may
451 involve feedbacks which can result in positive associations (as also seen in Mondal et al., 2020).

452 In addition, our results clearly underline the complexity and non-linearity between
453 aerosol, VPD and EF, and provides observational evidence to the discussions reported in Steiner
454 et al., 2011; 2013. Keeping all other factors relatively constant, increase in scattering aerosols
455 causes a positive AOD-EF association (as seen in HALT). In case of HAHT, as both AOD and
456 VPD increased in phase over the week, VPD-induced reduction in evapotranspiration
457 compensated a major portion of the aerosol fertilization effect resulting in a slight increase in
458 latent heat with increase in AOD. Also note that, combined effect of increase in AOD and T_{air}
459 caused a large suppression in sensible heat fluxes. Thus, EF also increases with AOD under
460 heatwave conditions. However, in absence of significant aerosol variation, the increase in VPD
461 causes a large reduction in evapotranspiration (as seen in LAHT). First, negligible aerosol
462 fertilization effect and second, increase in canopy resistance (via stomatal aperture reduction)
463 under steep rise in VPD values caused large reduction in latent heat across the week during
464 LAHT. High VPD is also linked with greater T_{air} during heatwave scenarios, thereby inducing
465 reduction the near surface temperature gradient and sensible heat during LAHT. Thus, both
466 sensible heat and latent heat release decreased with VPD causing negligible change in EF with
467 VPD. Thus, the VPD-EF coupling is very strong in absence of aerosol loading but weakens
468 under aerosol loading. Along with aerosol fertilization effect, the direct deposition of aerosols as
469 a wax layer on the leaf surface can also contribute to such an effect [Burkhardt., 2010; Burkhardt
470 and Grantz., 2017]. Recently, Grantz *et al.* 2018 used direct observations in glasshouses to
471 illustrate decoupling of stomata conductance (flux-based) from its porosity (higher VPD induces
472 reduction in pore size) under more aerosol scenario. India's mean temperature is constantly
473 rising [Krishnan et al., 2020]. At the same time, the global mean VPD is increasing with global
474 warming [Yuan et al., 2019] and heatwaves will be more frequent in future India [Mukherjee et
475 al., 2018]. Moreover, anthropogenic emissions over Indian Subcontinent will ensure high AOD

476 values in near future [Kumar et al 2018], thus manifesting a HAHT-like scenario at longer time
477 scales over India. Although, the response of plants and crops to enhancement in VPD in warmer
478 future is uncertain, but aerosol-induced weakening of VPD-EF associations can contribute
479 towards tendency of crops and vegetations becoming less drought/heat-resilient in future.

480

481

482 **6. Summary**

483

484 In summary, simultaneous observations from AERONET and an eddy covariance flux tower
485 equipped with micrometeorological and soil physics sensors were employed to report possible
486 influence of aerosol loading on VPD-Evaporative Fraction associations over a natural C4
487 grassland site under clear sky conditions in the central Gangetic Plains. The main findings from
488 this study are:

489

- 490 1. Increase in aerosol loading reduces the incoming solar radiation at surface and reduces
491 the gradient between surface temperature and near-surface air temperature. This is
492 associated with the decrease in energy dissipation from surface via sensible heat. At the
493 same time, increase in aerosol loading increases the evapotranspiration efficiency of
494 ecosystem by increasing diffuse radiation. Thus, high aerosol loading favors dissipation
495 of available surface energy via Latent heat flux and therefore increases Evaporative
496 fraction.
- 497 2. Increase in surface temperature and VPD during heatwave conditions induce larger
498 canopy resistance and stomata closure, thereby reducing the LH fluxes and EF. Native
499 Plants tend to store more water by transpiring less in high temperature conditions; so GPP
500 (and thus LH) reduces under high temperatures. At the same time, higher air temperature,
501 also reduces the sensible heat partitioning via reduction in near surface temperature
502 gradient. Thus, as the effect of VPD involves reducing both the surface fluxes, the net
503 effect on EF is negligible.
- 504 3. The variability in aerosol loading tends to play a significant role in modulating the VPD-
505 EF association under varying VPD/surface temperature. When the changes in VPD and
506 scattering aerosols are in phase, like in case of stagnant heat wave conditions over North

507 India, the VPD-induced reduction in evapotranspiration may be completely compensated.
508 This physiological changes can be due to the aerosol fertilization effect or thick aerosol
509 deposition/coating on leaves. Besides, as both increasing AOD and T_{air} induces
510 suppression in sensible heat partitioning, largely the changes in net EF remains in phase
511 with changes in AOD and VPD.

512
513 Nonetheless, a few caveats of this study need to be kept in mind. Our analysis, although driven
514 by fundamental theory of land-atmosphere interactions, is statistical in nature with a relatively
515 small sample size. The cases we analyse here and carefully selected to represent the distinct
516 scenarios as far as realistically possible in this region. Thus, minor influences of meteorological
517 co-variability cannot be totally avoided. As such, the quantitative estimation of various
518 associations may have inherent uncertainties and care should be taken before generalizing.
519 Moreover, as literature on plant physiological responses specific to grass variants found in the
520 Indo-Gangetic Basin region are scarce, this study warrants more species-level studies are
521 necessary to isolate the physiological and environmental responses on EF. Nevertheless, the
522 possible AOD-VPD-EF associations discussed here can have substantial implications on future
523 climate of this and similar subtropical regions. Thus, the observational associations provided in
524 this study not only encourages more measurements, detailed in situ experiments and mechanistic
525 modelling of aerosol-vegetation-atmosphere interactions, but also warrants proper
526 representations of aerosol processes and feedbacks in coupled models over India.

527

528 **Acknowledgement:**

529 SNT gratefully acknowledge the financial support given by the Earth System Science
530 Organization, Ministry of Earth Sciences, Government of India (grant MM/NERC-MoES-
531 03/2014/002) and Newton Fund to conduct this research under Monsoon Mission. CS
532 acknowledges support from MHRD, India under project number SB20210835CEMHRD00850.
533 LMM acknowledges the support of the Natural Environment Research Council (NERC) South
534 American Biomass Burning Analysis (SAMBBA) project grant code NE/J010057/1. The authors
535 would like to thank Dr E. J. Welton, B.N. Holben and staff at NASA GSFC for establishing and
536 quality control of the AERONET and MPLNET site at IIT Kanpur, used in this study.

537

538 **Data statement:**

539 Surface data used here is available at: [https://catalogue.ceh.ac.uk/documents/78c64025-1f8d-](https://catalogue.ceh.ac.uk/documents/78c64025-1f8d-431c-bdeb-e69a5877d2ed)
540 [431c-bdeb-e69a5877d2ed](https://catalogue.ceh.ac.uk/documents/78c64025-1f8d-431c-bdeb-e69a5877d2ed). Aerosol data used here is available from
541 <https://www.iitk.ac.in/ce/aeronet>.

542

543

544

545

546 **References**

- 547 1. Bollasina, M. A., and Y. Ming (2013), The role of land-surface processes in modulating
548 the Indian monsoon annual cycle, *Climate Dynamics*, 41(9-10), 2497-2509.
- 549 2. Campbell, J. R., D. L. Hlavka, E. J. Welton, C. J. Flynn, D. D. Turner, J. D. Spinhirne, V.
550 S. S. III, and I. H. Hwang (2002), Full-Time, Eye-Safe Cloud and Aerosol Lidar
551 Observation at Atmospheric Radiation Measurement Program Sites: Instruments and Data
552 Processing, *Journal of Atmospheric and Oceanic Technology*, 19(4), 431-442.
- 553 3. Chakraborty, S., U. Saha, and A. Maitra (2015), Relationship of convective precipitation
554 with atmospheric heat flux — A regression approach over an Indian tropical location,
555 *Atmospheric Research*, 161–162, 116-124.
- 556 4. Chameides, W. L., et al. (1999), Case study of the effects of atmospheric aerosols and
557 regional haze on agriculture: An opportunity to enhance crop yields in China through
558 emission controls?, *Proceedings of the National Academy of Sciences*, 96(24), 13626-
559 13633.
- 560 5. Collatz, G. J., J. T. Ball, C. Grivet, and J. A. Berry (1991), Physiological and
561 environmental regulation of stomatal conductance, photosynthesis and transpiration: a
562 model that includes a laminar boundary layer, *Agricultural and Forest Meteorology*, 54(2),
563 107-136.
- 564 6. Dey, S., and L. Di Girolamo (2011), A decade of change in aerosol properties over the
565 Indian subcontinent, *Geophysical Research Letters*, 38(14), n/a-n/a.
- 566 7. Dimitris, G. K., P. S. Ramesh, G. Ritesh, S. Manish, P. G. Kosmopoulos, and S. N.
567 Tripathi (2012), Variability and trends of aerosol properties over Kanpur, northern India
568 using AERONET data (2001–10), *Environmental Research Letters*, 7(2), 024003.
- 569 8. Forster, P., V. Ramaswamy, P. Artaxo, T. Berntsen, R. Betts, D. W. Fahey, J. Haywood, J.
570 Lean, D. C. Lowe, and G. Myhre (2007), Changes in atmospheric constituents and in
571 radiative forcing. Chapter 2, in *Climate Change 2007. The Physical Science Basis*, edited.
- 572 9. Gautam, R., N. C. Hsu, and K. M. Lau (2010), Premonsoon aerosol characterization and
573 radiative effects over the Indo-Gangetic Plains: Implications for regional climate
574 warming, *Journal of Geophysical Research: Atmospheres*, 115(D17), n/a-n/a.
- 575 10. Gautam, R., et al. (2011), Accumulation of aerosols over the Indo-Gangetic plains and
576 southern slopes of the Himalayas: distribution, properties and radiative effects during the
577 2009 pre-monsoon season, *Atmos. Chem. Phys.*, 11(24), 12841-12863.
- 578 11. Gu, L., T. Meyers, S. G. Pallardy, P. J. Hanson, B. Yang, M. Heuer, K. P. Hosman, J. S.
579 Riggs, D. Sluss, and S. D. Wullschleger (2006), Direct and indirect effects of atmospheric

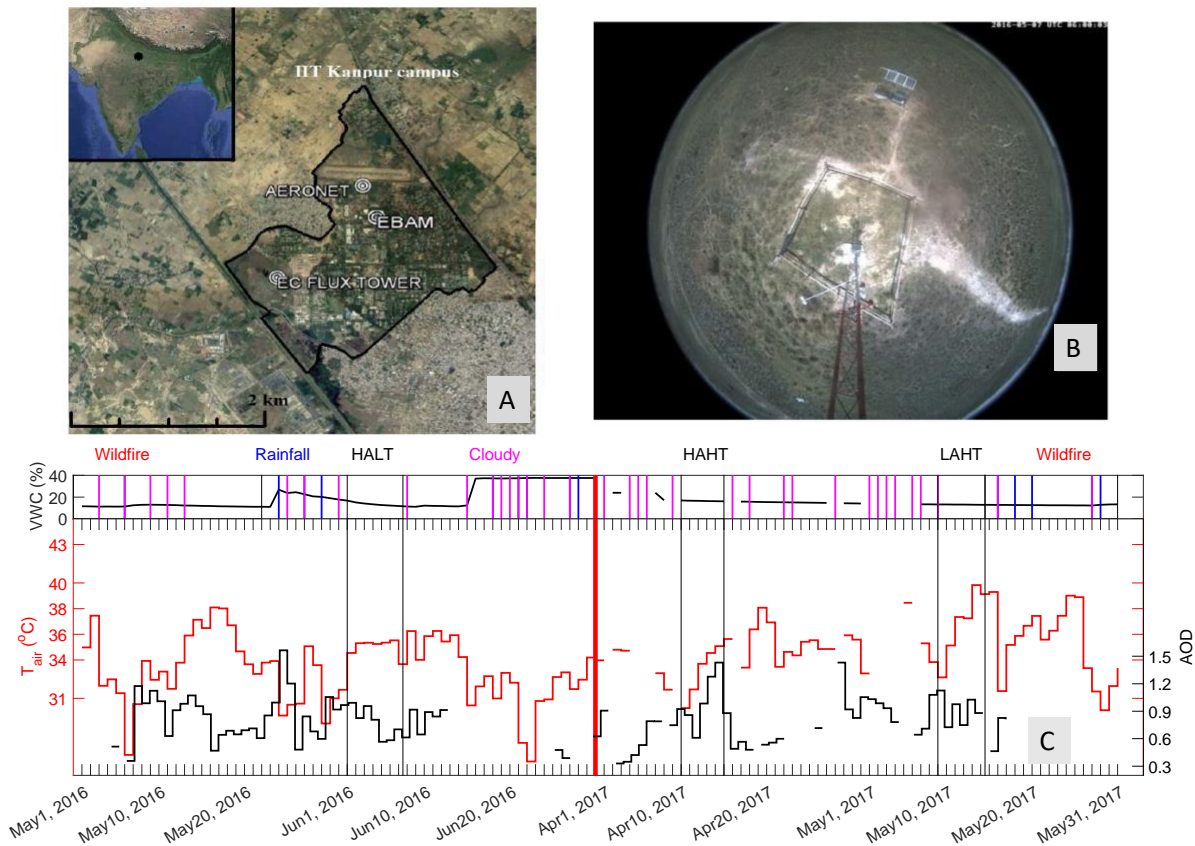
- 580 conditions and soil moisture on surface energy partitioning revealed by a prolonged
581 drought at a temperate forest site, *Journal of Geophysical Research: Atmospheres*,
582 111(D16), n/a-n/a.
- 583 12. Jones, H. G., and R. A. Sutherland (1991), Stomatal control of xylem embolism, *Plant*,
584 *Cell & Environment*, 14(6), 607-612.
- 585 13. Liu, S., M. Chen, and Q. Zhuang (2014), Aerosol effects on global land surface energy
586 fluxes during 2003–2010, *Geophysical Research Letters*, 41(22), 7875-7881.
- 587 14. Mallet, M., P. Tulet, D. Serça, F. Solmon, O. Dubovik, J. Pelon, V. Pont, and O. Thouron
588 (2009), Impact of dust aerosols on the radiative budget, surface heat fluxes, heating rate
589 profiles and convective activity over West Africa during March 2006, *Atmos. Chem.*
590 *Phys.*, 9(18), 7143-7160.
- 591 15. Matsui, T., A. Beltrán-Przekurat, D. Niyogi, R. A. Pielke, and M. Coughenour (2008),
592 Aerosol light scattering effect on terrestrial plant productivity and energy fluxes over the
593 eastern United States, *Journal of Geophysical Research: Atmospheres*, 113(D14), n/a-n/a.
- 594 16. Murthy, B. S., R. Latha, K. Manoj, and N. C. Mahanti (2014), Effect of aerosols on
595 evapo-transpiration, *Atmospheric Environment*, 89, 109-118.
- 596 17. Niyogi, D., H.-I. Chang, F. Chen, L. Gu, A. Kumar, S. Menon, and R. A. Pielke (2007),
597 Potential impacts of aerosol–land–atmosphere interactions on the Indian monsoonal
598 rainfall characteristics, *Natural Hazards*, 42(2), 345-359.
- 599 18. Niyogi, D., et al. (2004), Direct observations of the effects of aerosol loading on net
600 ecosystem CO₂ exchanges over different landscapes, *Geophysical Research Letters*,
601 31(20), n/a-n/a.
- 602 19. Pandithurai, G., C. Seethala, B. S. Murthy, and P. C. S. Devara (2008a), Investigation of
603 atmospheric boundary layer characteristics for different aerosol absorptions: Case studies
604 using CAPS model, *Atmospheric Environment*, 42(19), 4755-4768.
- 605 20. Pandithurai, G., S. Dipu, K. K. Dani, S. Tiwari, D. S. Bisht, P. C. S. Devara, and R. T.
606 Pinker (2008b), Aerosol radiative forcing during dust events over New Delhi, India,
607 *Journal of Geophysical Research: Atmospheres*, 113(D13), n/a-n/a.
- 608 21. Saha, S. K., S. Halder, K. K. Kumar, and B. N. Goswami (2011), Pre-onset land surface
609 processes and ‘internal’ interannual variabilities of the Indian summer monsoon, *Climate*
610 *Dynamics*, 36(11), 2077-2089.
- 611 22. Sarangi, C., S. N. Tripathi, A. K. Mishra, A. Goel, and E. J. Welton (2016), Elevated
612 aerosol layers and their radiative impact over Kanpur during monsoon onset period,
613 *Journal of Geophysical Research: Atmospheres*, 121(13), 7936-7957.
- 614 23. Schwartz, S. E. (1996), Atmospheric Aerosols The whitehouse effect—Shortwave
615 radiative forcing of climate by anthropogenic aerosols: an overview, *Journal of Aerosol*
616 *Science*, 27(3), 359-382.
- 617 24. Srivastava, A., S. Tiwari, P. Devara, D. Bisht, M. K. Srivastava, S. Tripathi, P. Goloub,
618 and B. Holben (2011), Pre-monsoon aerosol characteristics over the Indo-Gangetic Basin:
619 implications to climatic impact, paper presented at *Annales Geophysicae*, European
620 Geosciences Union.
- 621 25. Steiner, A. L., and W. L. Chameides (2011), Aerosol-induced thermal effects increase
622 modelled terrestrial photosynthesis and transpiration, *Tellus B*, 57(5).
- 623 26. Steiner, A. L., D. Mermelstein, S. J. Cheng, T. E. Twine, and A. Oliphant (2013),
624 Observed Impact of Atmospheric Aerosols on the Surface Energy Budget, *Earth*
625 *Interactions*, 17(14), 1-22.

- 626 27. Trenberth, K. E., J. T. Fasullo, and J. Kiehl (2009), Earth's Global Energy Budget,
627 Bulletin of the American Meteorological Society, 90(3), 311-323.
- 628 28. Urankar, G., T. V. Prabha, G. Pandithurai, P. Pallavi, D. Achuthavarier, and B. N.
629 Goswami (2012), Aerosol and cloud feedbacks on surface energy balance over selected
630 regions of the Indian subcontinent, Journal of Geophysical Research: Atmospheres,
631 117(D4), n/a-n/a.
- 632 29. Wang, K., and R. E. Dickinson (2012), A review of global terrestrial evapotranspiration:
633 Observation, modeling, climatology, and climatic variability, Reviews of Geophysics,
634 50(2), n/a-n/a.
- 635 30. Wang, K., R. E. Dickinson, and S. Liang (2008), Observational evidence on the effects of
636 clouds and aerosols on net ecosystem exchange and evapotranspiration, Geophysical
637 Research Letters, 35(10), n/a-n/a.
- 638 31. Welton, E. J., and J. R. Campbell (2002), Micropulse Lidar Signals: Uncertainty Analysis,
639 Journal of Atmospheric and Oceanic Technology, 19(12), 2089-2094.
- 640 32. Yu, H., S. C. Liu, and R. E. Dickinson (2002), Radiative effects of aerosols on the
641 evolution of the atmospheric boundary layer, Journal of Geophysical Research:
642 Atmospheres, 107(D12), AAC 3-1-AAC 3-14.
- 643 33. Koster, R. D., Dirmeyer, P. A., Guo, Z., Bonan, G., Chan, E., Cox, P., ... & Liu, P. (2004).
644 Regions of strong coupling between soil moisture and precipitation. *Science*, 305(5687),
645 1138-1140.
- 646 34. Turner, A. G., Bhat, G. S., Martin, G. M., Parker, D. J., Taylor, C. M., Mitra, A. K., ... &
647 Morrison, R. (2019). Interaction of convective organization with monsoon precipitation,
648 atmosphere, surface and sea: The 2016 INCOMPASS field campaign in India. *Quarterly*
649 *Journal of the Royal Meteorological Society*.
- 650 35. Chakraborty, T., & Lee, X. (2019). Land cover regulates the spatial variability of
651 temperature response to the direct radiative effect of aerosols. *Geophysical Research*
652 *Letters*, 46(15), 8995-9003.
- 653 36. Chakraborty, T., Sarangi, C., Krishnan, M., Tripathi, S. N., Morrison, R., & Evans, J.
654 (2019). Biases in model-simulated surface energy fluxes during the Indian monsoon onset
655 period. *Boundary-Layer Meteorology*, 170(2), 323-348.
- 656 37. Chakraborty, T. C., Lee, X., & Lawrence, D. M. (2021). Strong local evaporative cooling over
657 land due to atmospheric aerosols. *Journal of Advances in Modeling Earth Systems*, 13(5),
658 e2021MS002491.
- 659
- 660 38. Rigden, A. J., & Salvucci, G. D. (2017). Stomatal response to humidity and CO₂
661 implicated in recent decline in US evaporation. *Global Change Biology*, 23(3), 1140-
662 1151.
- 663 39. Yuan, W., Zheng, Y., Piao, S., Ciais, P., Lombardozzi, D., Wang, Y., ... & Jain, A. K.
664 (2019). Increased atmospheric vapor pressure deficit reduces global vegetation
665 growth. *Science advances*, 5(8), eaax1396.
- 666 40. Wang Z., C. Wang, B. Wang, X. Wang, J. Li, J. Wu, L. Liu Interactive effects of air
667 pollutants and atmospheric moisture stress on aspen growth and photosynthesis along an
668 urban-rural gradient. *Environ. Pollut.*, 260 (2020),
669 Article 114076, [10.1016/j.envpol.2020.114076](https://doi.org/10.1016/j.envpol.2020.114076)
- 670 41. Burkhardt J, Grantz DA. 2017. Plants and atmospheric aerosols. *Progress Botany* 78: 369-
671 406

- 672 42. Burkhardt J. 2010. Hygroscopic particles on leaves: nutrients or desiccants? *Ecological*
673 *Monographs***80**: 369– 399.
- 674 43. Grantz DA, Zinsmeister D, Burkhardt J. 2018. Ambient aerosol increases minimum leaf
675 conductance and alters the aperture–flux relationship as stomata respond to vapor pressure
676 deficit (VPD). *New Phytologist* **219**: 275– 286.
- 677 44. R. Latha, B. S. Murthy & B. Vinayak (2019) Aerosol-induced perturbation of surface
678 fluxes over different landscapes in a tropical region, *International Journal of Remote*
679 *Sensing*, 40:21, 8203-8221, DOI: [10.1080/01431161.2018.1523586](https://doi.org/10.1080/01431161.2018.1523586)
- 680 45. Krishnan et al (2020) Assessment of climate change over the Indian region: a report of the
681 Ministry of Earth Sciences (MoES), Government of India
- 682 46. WangX., J. Wu, M. Chen, X. Xu, Z. Wang, B. Wang, C. Wang, S. Piao, W. Lin, G. Miao,
683 Deng, C. Qiao, J. Wang, S. Xu, L. Liu, Field evidences for the positive effects of aerosols
684 on tree growth. *Global Change Biol.*, 24 (2018), pp. 4983-4992
- 685 47. Myhre, G., Samset, B.H., Hodnebrog, Ø. *et al.* Sensible heat has significantly affected the
686 global hydrological cycle over the historical period. *Nat Commun* **9**, 1922 (2018).
687 <https://doi.org/10.1038/s41467-018-04307-4>
- 688 48. Rao, K. G., & Reddy, N. N. (2019). On moisture flux of the Indian summer monsoon: A
689 new perspective. *Geophysical Research*
690 *Letters*, 46, 1794– 1804. <https://doi.org/10.1029/2018GL080392>
- 691 49. Mondal, A, Sah, N, Sharma, A, Venkataraman, C, Patil, N. Absorbing aerosols and
692 high-temperature extremes in India: A general circulation modelling study. *Int J*
693 *Climatology*. 2020; 1– 20. <https://doi.org/10.1002/joc.6783>
- 694 50. Shen Z, Ming Y, Held IM. Using the fast impact of anthropogenic aerosols on regional
695 land temperature to constrain aerosol forcing. *Sci Adv*. 2020 Aug 5;6(32): doi:
696 10.1126/sciadv.5297.
- 697 51. Dave P, Bhushan, M., Venkataraman, C., Absorbing aerosol influence on temperature
698 maxima: An observation-based study over India. *Atmospheric Environment*, Volume 223,
699 2020, 117237, ISSN 1352-2310, <https://doi.org/10.1016/j.atmosenv.2019.117237>.
- 700 52. Talukdar S. and M.V. Ratnam, A mutual response between surface temperature and black
701 carbon mass concentration during the daytime, *Science of the Total Environment*,
702 <https://doi.org/10.1016/j.scitotenv.2020.143477>
- 703 53. Knohl, A., and D. D. Baldocchi (2008), Effects of diffuse radiation on canopy gas
704 exchange processes in a forestecosystem, *J. Geophys. Res.*, 113, G02023,
705 doi:10.1029/2007JG000663
- 706 54. Davin, E. L. and Seneviratne, S. I.: Role of land surface processes and diffuse/direct
707 radiation partitioning in simulating the European climate, *Biogeosciences*, 9, 1695–1707,
708 <https://doi.org/10.5194/bg-9-1695-2012>, 2012
- 709 55. O’Sullivan, M., A. Rap, C. L. Reddington, D. V. Spracklen, M. Gloor, and W. Buermann
710 (2016), Small global effecton terrestrial net primary production due to increased fossil fuel
711 aerosol emissions from East Asia since the turnof the century, *Geophys. Res. Lett.*,
712 43,8060–8067, doi:10.1002/2016GL068965.
- 713 56. Yue, X. and Unger, N.: Aerosol optical depth thresholds as a tool to assess diffuse
714 radiation fertilization of the land carbon uptake in China, *Atmos. Chem. Phys.*, 17, 1329–
715 1342, <https://doi.org/10.5194/acp-17-1329-2017>, 2017.

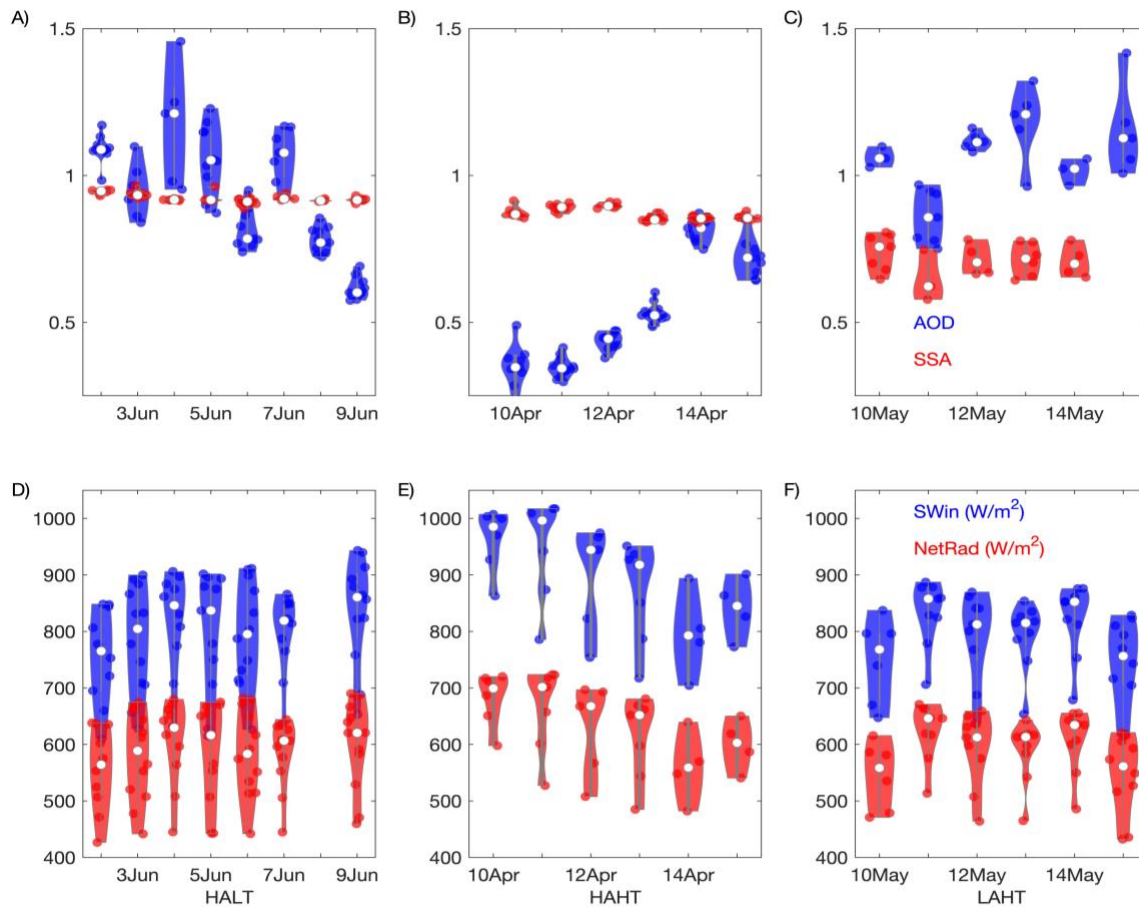
- 716 57. Mercado LM, Bellouin N, Sitch S, Boucher O, Huntingford C, Wild M, Cox PM. Impact
717 of changes in diffuse radiation on the global land carbon sink. *Nature*. 2009 Apr
718 23;458(7241):1014-7. doi: 10.1038/nature07949. PMID: 19396143.
- 719 58. Kumar, R., Barth, M. C., Pfister, G. G., Delle Monache, L., Lamarque, J. F., Archer-
720 Nicholls, S., Walters, S. (2018). How will air quality change in South Asia by
721 2050? *Journal of Geophysical Research:*
722 *Atmospheres*, 123, 1840– 1864. <https://doi.org/10.1002/2017JD027357>
- 723 59. M. Kumar, K.S. Parmar, D.B. Kumar, A.Mhawish, D.M. Broday, R.K. Mall, T. Banerjee
724 Long-term aerosol climatology over Indo-Gangetic Plain: trend, prediction and potential
725 source field; *Atmos. Environ.*, 180 (2018), pp. 37-50
- 726 60. Bhat G. S., R. Morrison, C. M. Taylor, B. K. Bhattacharya, S. Paler, D. Desai, J. G.
727 Evans, S. Pattnaik, M. Sekhar, R. Nigam, A. Sattar, S. S. Angadi, D. Kacha, A. Patidar, S.
728 N. Tripathi, K. V. M. Krishnan, A. Sisodiya; Spatial and temporal variability in energy
729 and water vapour fluxes observed at seven sites on the Indian subcontinent during 2017. *Q*
730 *J R Meteorol Soc.* 2020; 146: 2853– 2866. <https://doi.org/10.1002/qj.3688>
- 731 61. Ratnam, J., Behera, S., Ratna, S. *et al.* Anatomy of Indian heatwaves. *Sci Rep* 6, 24395
732 (2016). <https://doi.org/10.1038/srep24395>.
- 733 62. Mukherjee, S., Mishra, V. A sixfold rise in concurrent day and night-time heatwaves in
734 India under 2 °C warming. *Sci Rep* 8, 16922 (2018). <https://doi.org/10.1038/s41598-018-35348-w>
- 735 63. Morrison, R.; Angadi, S.S.; Cooper, H.M.; Evans, J.G.; Rees, G.; Sekhar, M.; Taylor, C.;
736 Tripathi, S.N.; Turner, A.G. (2019). Energy and carbon dioxide fluxes, meteorology and
737 soil physics observed at INCOMPASS land surface stations in India, 2016 to 2017. NERC
738 Environmental Information Data Centre. <https://doi.org/10.5285/78c64025-1f8d-431c-bdeb-e69a5877d2ed>
- 739 64. Mayank Gupta et al 2021 *Environ. Res. Lett.* 16 014021
- 740 65. Rohini, P., Rajeevan, M. & Srivastava, A. On the Variability and Increasing Trends of
741 Heat Waves over India. *Sci Rep* 6, 26153 (2016). <https://doi.org/10.1038/srep26153>
- 742 66. Mwendia, S. W., Yunusa, I. A., Sindel, B. M., Whalley, R. D., & Kariuki, I. W. (2017).
743 Assessment of Napier grass accessions in lowland and highland tropical environments of
744 East Africa: water stress indices, water use and water use efficiency. *Journal of the*
745 *Science of Food and Agriculture*, 97(6), 1953-1961.
- 746 67. van Heerwaarden, C. C., & Teuling, A. J. (2014). Disentangling the response of forest and
747 grassland energy exchange to heatwaves under idealized land–atmosphere
748 coupling. *Biogeosciences*, 11(21), 6159-6171.
- 749 68. Juan Andrés Cardoso, Marcela Pineda, Juan de la Cruz Jiménez, Manuel Fernando
750 Vergara, Idupulapati M. Rao, Contrasting strategies to cope with drought conditions by
751 two tropical forage C₄grasses, *AoB PLANTS*, Volume 7, 2015,
752 plv107, <https://doi.org/10.1093/aobpla/plv107>
- 753 69. Liang, X., Erickson, J.E., Sollenberger, L.E., Rowland, D.L., Silveira, M.L. and
754 Vermerris, W. (2018), Growth and Transpiration Responses of Elephantgrass and
755 Energycane to Soil Drying. *Crop Science*, 58: 354-
756 363. <https://doi.org/10.2135/cropsci2017.01.0019>
- 757 70. Purbajanti, E.; Anwar, S.; Wydiati, F.K. Drought stress effect on morphology characters,
758 water use efficiency, growth and yield of guinea and napier grasses. *Int. Res. J. Plant*
759 *Sci.* 2012, 3, 47. [[Google Scholar](#)]

762 71. Mwendia, S.; Yunusa, I.; Whalley, R.; Sindel, B.; Kenney, D.; Kariuki, I. Use of plant water
763 relations to assess forage quality and growth for two cultivars of Napier grass (*Pennisetum*
764 *purpureum*) subjected to different levels of growth of soil water supply and temperature regimes. *Crop*
765 *Pasture Sci.* **2014**, *64*, 1008–1019. [[Google Scholar](#)]
766 72. Holm L, Pancho JV, Herberger JP, Plucknett DL, 1979. A Geographical Atlas of World
767 Weeds. Toronto, Canada: John Wiley and Sons Inc
768 73. Charlotte Grossiord, Thomas N. Buckley, Lucas A. Cernusak, Kimberly A.
769 Novick, Benjamin Poulter, Rolf T. W. Siegwolf, John S. Sperry, Nate G. McDowell
770 74. Irmak, S., and Mutiibwa, D. (2010), On the dynamics of canopy resistance: Generalized
771 linear estimation and relationships with primary micrometeorological variables, *Water*
772 *Resour. Res.*, 46, W08526, doi:[10.1029/2009WR008484](https://doi.org/10.1029/2009WR008484).
773
774
775
776



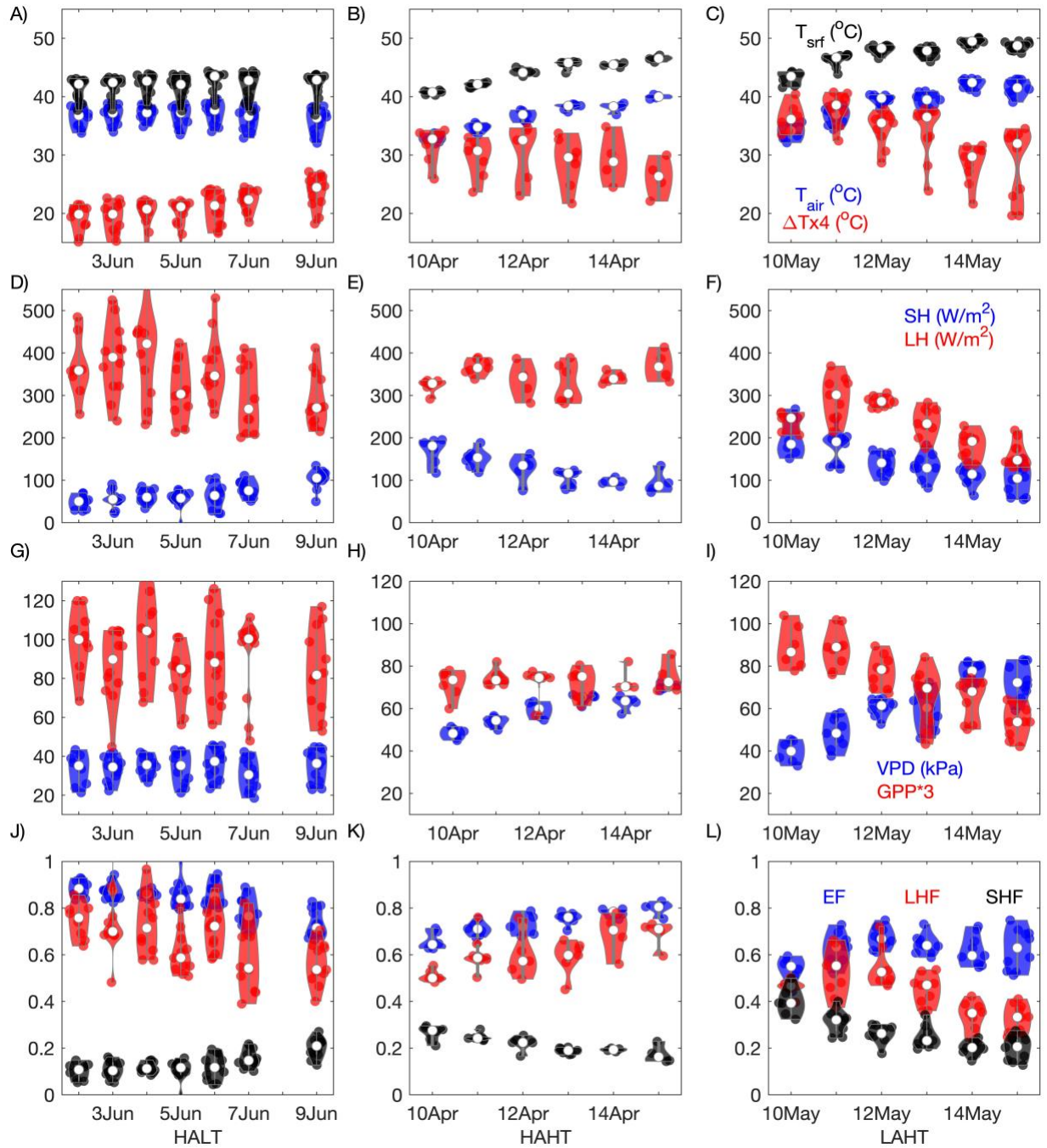
777
778 *Figure 1: A) Map showing the locations of AERONET and the EC flux tower site within the*
779 *campus of the Indian Institute of Technology Kanpur (IITK). Inset map shows the location of*
780 *IITK (black dot) in the central Gangetic Plains. The maps are created by © Google Maps 2017.*
781 *B) Camera image of land cover of the flux tower site during May 12th, 2017. C) Daily variation*
782 *in soil moisture (VWC, volumetric water content) during our study period is shown in black line*

783 in upper box of the figure. The occurrences of cloudy days, rainy days and wildfire affected
 784 period during April through June of 2016 and 2017 is shown by magenta, blue and pink colour
 785 patches in the upper box. A cloudy day is inferred from MPLNET images and AERONET
 786 observations (as defined in Section 2 of main text). The days bounded by straight lines depict the
 787 weekly episodes HALT, HAHT and LAHT, respectively. Daily variation in T_{air} and daily
 788 variation in AOD during our study period is shown as black and red lines in lower box of the
 789 panel.
 790



791
 792 *Figure 2: Distribution plots showing the variations in aerosol and radiation during the cases.*
 793 *Row 1 illustrates Time series of midday (1100-1400 LT) variation in AOD and SSA values*
 794 *during HALT, HAHT and LAHT, respectively.. The horizontal line within box represents median*
 795 *of the distribution. The bottom and top edge of the boxes represent 25th and 75th percentile,*
 796 *respectively, of the distribution. The short dash at top and bottom extent of the boxes represent*
 797 *5th and 95th percentile, respectively. Row 2 is same as Row 1 but show measurements of*
 798 *incoming short wave radiation and net radiation at surface. Note that June, 16 means June of*
 799 *2016 and so on.*

800
 801

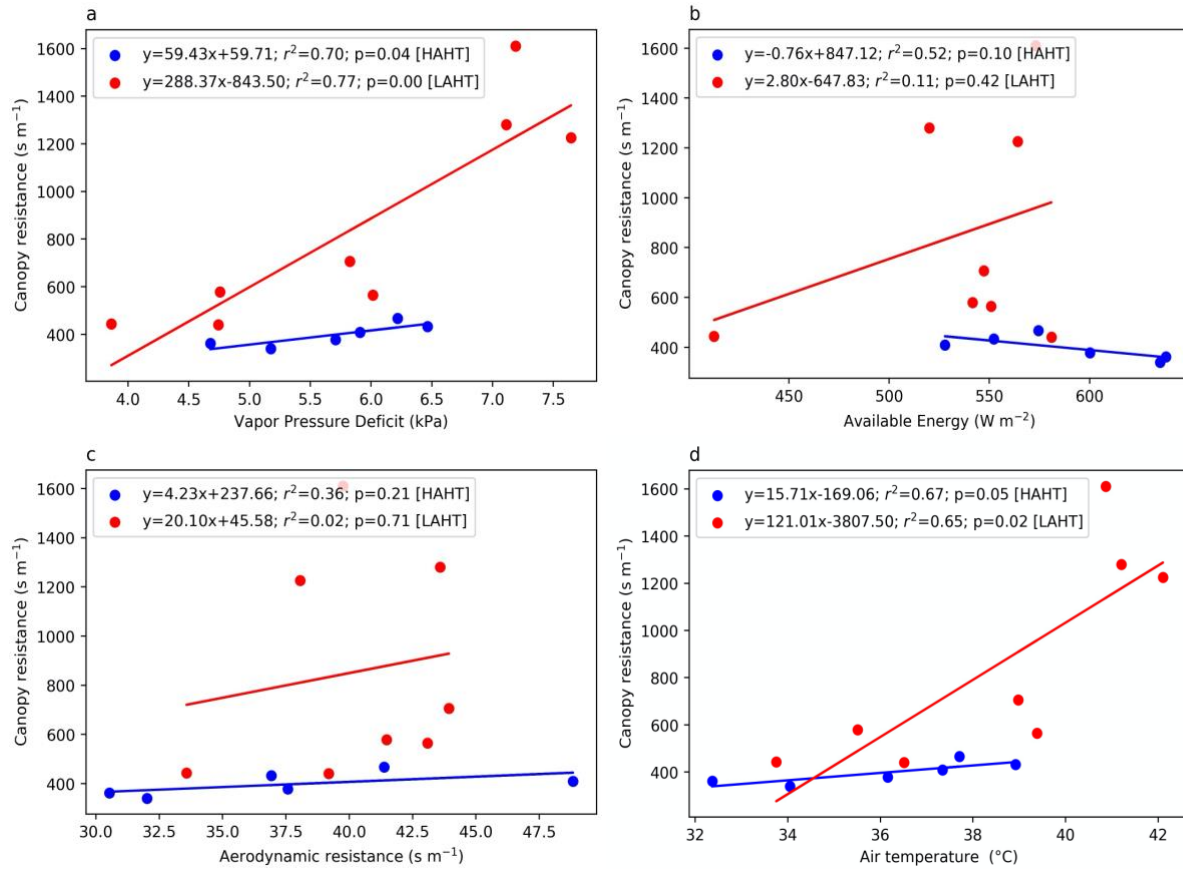


802

803 *Figure 3: Distribution plots showing the variations in near surface meteorology and surface*
 804 *fluxes during the cases. Row 1 illustrates Time series of midday (1100-1400 LT) variation in T_{srf} ,*
 805 *T_{air} and $(-)\Delta T$ values during HALT, HAHT and LAHT, respectively. Row 2 is same as Row 1 but*
 806 *for SH and LH. Row 3 is same but for VPD and GPP ; Row 4 is same but for EF, LHF (red) and*
 807 *SHF.*

808

809



810

811 *Figure 4: Linear correlation between daily midday average Canopy resistance derived from*
 812 *Penman-Monteith equation with a) observed Vapor Pressure Deficit (VPD); b) Available energy*
 813 *at surface; c) Aerodynamic resistance and d) Air temperature for HAHT and LAHT cases.*

814

815

816

817

818

819

820

821

822

823

824

825

826

827

Appendix A: Table of Abbreviations

Name	Abrv. used
Latent heat flux	LH
Sensible heat flux	SH
Ground heat flux	GH
Evaporative Fraction	EF
2 m air temperature	T _{air}
vapor pressure deficit	VPD
gross primary production	GPP
net radiation	NR
aerosol direct radiative effect	ADRE
aerosol diffuse radiation fertilization effect	ADFE
diffuse radiation	diffuse _{frac}
Santa Barbara discrete ordinates radiative transfer Atmospheric Radiative Transfer Model	SBDART
Aerosol RObotic NETwork	AERONET
Volumetric soil water content	VWC
surface temperature	T _{srf}
relative humidity	RH
Aerosol Optical Depth	AOD
Single Scattering Albedo	SSA
High AOD-Low T _{air}	HALT
High AOD-High T _{air}	HAHT
Low AOD- High T _{air}	LAHT
Outgoing long wave radiation at surface	LW _{out}
canopy resistance	r _s
aerodynamic resistance to heat transfer	r _a
Sensible heat fraction	SHF
Latent heat fraction	LHF

828